Experimental and (first-order many-body) theoretical differential and integral cross sections for excitation of the $n = 3$ states of He by electron impact at 29.2 and 39.7 eV

Ara Chutjian
Physics Section, Jet Propulsion Laboratory, California Institute of Technology, Pasadena, California 91103

Lowell D. Thomas
IBM Research Laboratory, Monterey and Cottle Roads, San Jose, California 95193
(Received 11 December 1974)

Differential and integral electron scattering cross sections have been measured and calculated for the transitions $1\,^1S \rightarrow 3\,^1S$, $3\,^3S$, $3\,^3P$ and for the experimentally unresolved transitions $1\,^1S \rightarrow 3\,^1P$, $3\,^{1,3}D$ in helium. Measurements were made relative to both the $2\,^3P$ and $2\,^1P$ transitions at incident electron energies of 29.2 and 39.7 eV, and over the angular range 5–136°. The $n = 3$ relative differential cross sections (DCS) were normalized to the absolute scale by utilizing known normalized absolute DCS for the $2\,^3P$ and $2\,^1P$ transitions. The theoretical calculations were carried out in the first-order many-body theory of Csanak, Taylor, and Yaris. Comparisons are also made of the present measurements and calculations with other calculations carried out for the $3\,^1S$, $3\,^1D$, and $3\,^1P$ states in the Born and several Ochkur-like approximations. The theoretical origins in several theories of the intriguing sharp minimum in the $1\,^1S \rightarrow 3\,^1S$ DCS are discussed.

I. INTRODUCTION

The study of low-to-intermediate-energy electron scattering from the helium atom is of interest from both an experimental and theoretical point of view. Helium is an important component of several different types of plasma media, such as the He-Ne laser, the Jovian atmosphere, and a variety of gas discharges. Electrons of energies less than 50 eV are present in these media, and it is desirable to know accurate differential and integral cross sections for inelastic e-He scattering in order to understand these often complex plasma environments. Partly as a result of this need, a large body of experimental measurements has recently become available on electron scattering to the $n = 2$ ($2\,^{1,3}S$, $2\,^{1,3}P$) states of helium. These include differential cross-section (DCS) measurements,[1-4] as well as integral electron-impact (excitation function) cross-section measurements[5] for the $n\,^1P$ states ($n = 2$, 3, and 4).

Theoretically, the e-He system at electron energies of 30–50 eV presents an infinity of open inelastic and ionization channels, so that an exact, close-coupling solution to the problem is not feasible. This system is thus a valuable "testing ground" for approximate theories which consider only a small number of the possible open channels. In particular, for the $n = 2$ states, the first-order many-body theory (FOMBT)[6] or random-phase approximation (RPA) was shown[7] to give correct predictions at incident electron energies of 30 eV and above, of the shape and magnitude of the DCS of singlet transitions, and good agreement in shape, but only qualitative agreement in magnitude, for triplet transitions. These results were in contrast to those of other first-order theories such as the Born, Glauber, and Ochkur-like which in this low-to-intermediate energy range generally gave unsatisfactory results in both shape and magnitude, especially for optically forbidden singlet and triplet transitions.[1,2]

An extension of the FOMBT to calculations in the $n = 3$ manifold represents a further critical test of the theory. At first blush, one would expect channel couplings to become increasingly important, and first-order theories to become less reliable since (i) the states in the $n = 3$ manifold are closer together in energy, and there are more of them; (ii) the $n = 2$ manifold lies below, with much larger excitation cross sections; (iii) the measurements of the present work were made at energies ~2 eV closer to threshold for the $n = 3$ states than the measurements of the $n = 2$ transitions.[1-3] Surprisingly, as the theoretical results presented here will show, the agreement between theory and experiment is as good, and in some cases better, than was found for the $n = 2$ case.[7] This encouraging result implies that the FOMBT contains many of the important physical effects operating in the e-He system at these electron energies.

We report here the first measurements of normalized absolute differential and integral scattering cross sections from the He $1\,^1S$ ground state to the $3\,^1S$, $3\,^3S$, $3\,^3P$, and to the combined (unresolved) $3\,^1P$, $3\,^{1,3}D$ states. Measurements were made at incident electron energies E_0 of 29.2 eV and 39.7 eV, and at scattering angles θ between 5° and 136°. The theoretical differential and integral scattering cross sections calculated in the FOMBT

are reported at each experimental E_0 and θ. Comparisons are made of the present experiments and calculations to the results of the Born and several Ochkur-like calculations[8] for the $3\,^1S$, $3\,^1D$, and $3\,^1P$ states, and to recent plane-wave exchange scattering amplitude calculations[9] for the $1\,^1S \rightarrow 3\,^3S$ transition.

In Sec. II the experimental techniques, method of conversion to the absolute scale, and sources of experimental error are discussed. In Sec. III a brief presentation of the important features of the first-order many-body theory is given. In Sec. IV the results of the experimental measurements and theoretical calculations are given in both tabular form and in figures. In this same section the results are discussed, and compared to the DCS of the $n=2$ states and also to other available integral cross-section measurements of the $n=3$ transitions.

II. EXPERIMENTAL METHODS

The experimental difficulties in the measurements of the differential cross sections to the $n=3$ states of He lie in the fact that (i) the excitation cross sections to these states is of the order of $(\frac{2}{3})^3 \sim 0.3$ of the DCS for excitation to the $n=2$ states; (ii) while the $n=2$ manifold consists of *four* electronic states lying within a 1.4-eV range of one another, the $n=3$ manifold consists of *six* states lying within 0.3 eV of one another. These difficulties were met in the present work by the use of a spectrometer having a low background count rate (~3–5 counts/min), enabling one to accumulate spectra for as long as 36 h, and to measure cross sections as small as 2×10^{-21} cm^2/sr. The apparatus resolution was sufficient to separate the $3\,^3P$ and $3\,^1P$ states from one another (0.080-eV separation), but not the $3\,^3D$ and $3\,^1D$ states from the $3\,^1P$ state (0.014- and 0.013-eV separation, respectively).

A. Description of the apparatus and method of data collection

The electron scattering spectrometer used in the present work was the same as used in previous measurements of the DCS of the $n=2$ states of He[1,2] and has been described in detail previously.[10] Briefly, a monoenergetic beam of electrons is focused onto a He atomic beam issuing from a multichannel capillary array source. The scattered electrons are energy analyzed and detected as a function of scattering angle over the range $-30° \leq \theta \leq 136°$. The detected electron counts are accumulated in a multichannel scaler as a function of energy loss, and the final spectrum recorded on paper tape and as an X-Y recorder plot. The spectra were recorded at resolutions varying from 0.042 to 0.055 eV (FWHM).

A series of energy-loss spectra recorded at angles between $\theta=30°$ and 136° at $E_0=29.2$ eV is shown in Fig. 1. In recording such spectra, the analyzer first swept through the energy-loss region of the $1\,^1S \rightarrow 2\,^3P$ and $2\,^1P$ transitions. It then "jumped" to the energy-loss range of the $n=3$ transitions. This jump feature eliminated the unnecessary accumulation of background spectra in the region between the last $n=2$ member ($2\,^1P$) and the first $n=3$ member ($3\,^3S$)—a region 1.5 eV long.

Accurate absolute DCS at incident energies very close to those of the present work were available for the $2\,^3P$ and $2\,^1P$ excitations from previous measurements of Refs. 1 and 2. A comparison of the peak heights of the $n=3$ transitions relative to those of the $2\,^3P$ and $2\,^1P$ transitions then placed the $n=3$ excitations on the absolute scale. The small difference between the present electron

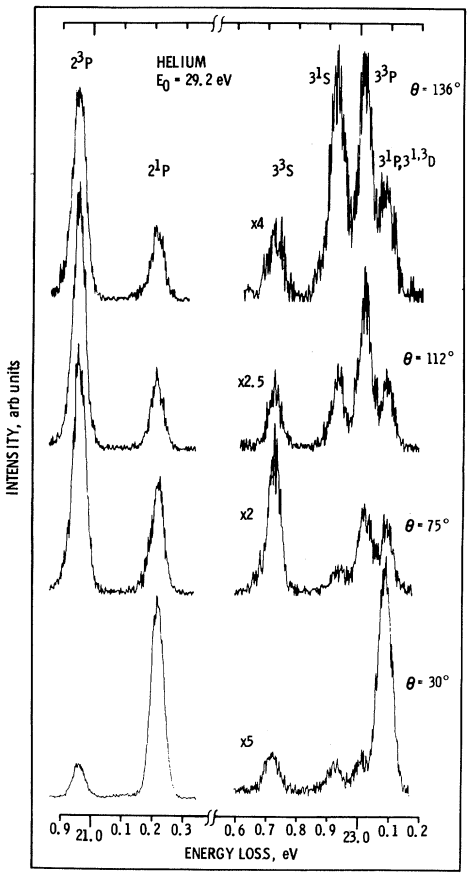

FIG. 1. Energy-loss spectra of helium at the incident electron energy $E_0=29.2$ eV, and at the scattering angles θ specified. Shown are the $n=3$ transitions, and the $2\,^{1,3}P$ transitions through which the $n=3$ transitions were normalized to the absolute scale.

energies (29.2 and 39.7 eV) and those of the $2^{1,3}P$ measurements (29.6 and 40.1 eV) was taken into account by multiplying the $2^{1,3}P$ DCS of Refs. 1 and 2 by the factors 0.947 and 0.985 at 29.6 and 40.1 eV, respectively. These factors were obtained from the integral cross-section measurements of Ref. 5 against which the $2^{1,3}P$ DCS were normalized.

B. Sources of experimental error

The major sources of error in the differential and integral cross-section measurements can be broken down into the sequence: (a) errors arising in the measurement of the intensity ratios between the $n=3$ excitations and $2\,^3P$ and $2\,^1P$ excitations. These errors include statistical errors due to the sometimes small number of counts accumulated in a particular feature, and errors due to partial blending of the $3\,^3P$ transition with the wings of the combined $3\,^1P$, $3^{1,3}D$ excitation at $\theta \leq 20°$; (b) errors in placing the measured intensity ratios on the absolute scale, which introduces the errors of the $2\,^3P$ and $2\,^1P$ DCS[1,2]; (c) extrapolation errors to $\theta = 0°$ and 180° in obtaining the integral cross sections for the $n=3$ excitations. Errors arising from the energy dependence of the analyzer optics and detector are considered negligible.[10] Other errors, such as the variation in He flow rate, incident electron current, or variation of the scattering volume with θ cancel out by virtue of the multichannel scaling technique, and the use of intensity ratios in the final spectrum.

1. Errors in the intensity ratios

The measure of intensity used was peak heights of the $n=3$ transitions relative to the peak heights of the $2\,^3P$ and $2\,^1P$ excitations. The error encountered in the use of peak heights, rather than areas, was checked at several angles at both incident energies, and the agreement between the two methods was found to be within 10%. Some blending was encountered at scattering angles at and below 20° between the $3\,^3P$ excitation and the combined $3\,^1P$, $3^{1,3}D$ excitations. At these scattering angles, the $3\,^3P$ intensity is less than 0.02 that of its $3\,^1P$, $3^{1,3}D$ neighbors, so that the wings of the stronger excitations tended to obscure the $3\,^3P$ excitation. A deconvolution scheme[11] was used in this case to help separate the transitions. For the purposes of the deconvolution, the $3^{1,3}D$ states were assumed to be superimposed on the $3\,^1P$ state. This is reasonable, since the D states lay within $\frac{1}{3}$–$\frac{1}{4}$ the instrumental width of the $3\,^1P$ state. The deconvolution routine assumed a Gaussian line profile, with the width of the profile measured from the stronger, isolated features in the $n=2$ spectrum. Several iterations about the specified width and peak-energy locations were carried out, and the iteration giving the best fit, in a least-squares sense, between the measured and calculated spectrum was used.

Also, the deconvolution routine was used to calculate the relative intensities within the $n=3$ manifold in all the spectra. This served as an independent check on the intensity ratios as read directly from the spectra. Finally, several sets of spectra were taken at the same scattering angle and incident electron energy, at intervals of several weeks and months, and the results averaged together. This was especially helpful in cases where the DCS dropped to less than 4×10^{-21} cm^2/sr, where the statistical error in the number of

TABLE I. Estimate of errors associated with the relative intensities of Tables II and III, and with the differential cross sections of Tables IV, V, Figs. 2, 3, and 5–10.

Source of error	Estimate of error (%) Angular range (deg) 0–20	21–90	91–136
Error in the intensity ratio DCS ($n=3$)/DCS($2\,^1P$ or $2\,^3P$), including statistical variation in the number of counts	15(20) [a]	15(30) [b]	15(20) [c]
Error in the DCS ($2\,^1P$) [d]	18	15	18
Error in the DCS ($2\,^3P$) [d]	20	14	18
Total rms error in the DCS ($n=3$)	25(28) [a]	21(34) [b]	23(27) [c]

[a] Larger error refers to the $3\,^3P$ excitation which is obscured by the wings of the $3\,^1P$, $3^{1,3}D$ excitations at scattering angles ≤ 20°.

[b] Larger error refers to the weak $3\,^1S$ excitation between 21° and 90°.

[c] Larger error refers to the weak $3\,^3S$ excitation between 105° and 136°.

[d] Reference 1. The larger of the $2\,^1P$ and $2\,^3P$ errors was used to obtain the rms error in the DCS ($n=3$). Also, the larger errors covering the angular range (0–10)° of Ref. 1 were applied to the (0–20)° range here.

counts was in the range (20–30)%. The errors in the intensity ratios in several angular ranges are summarized in Table I.

2. Errors in conversion to normalized absolute differential cross sections

The effect of including *both* the $2\,^3P$ and $2\,^1P$ transitions in each spectrum (see Fig. 1) was to maintain a constant statistical error over the entire angular range of the measurements. Thus, while the $2\,^1P$ DCS is dropping rapidly with increasing angle,[2] the $2\,^3P$ DCS is relatively flat,[1] and is a factor of 2–4 that of the $2\,^1P$ DCS for angles greater than about 80°. Also, the fact that one obtains two independent sets of intensity ratios in each spectrum results in a reduction of the over-all error in the DCS over that which would arise if only one $n=2$ transition were included.

An estimate of the errors in the measurements of the $2\,^3P$ and $2\,^1P$ DCS is given in Ref. 1, Table VI. These errors are listed in Table I, along with the root-mean-square error in the present measurements of the DCS of the $n=3$ transitions.

3. Errors in the integral cross sections

The primary source of error in the integral cross section of each $n=3$ transition is the error in the respective DCS itself, listed in Table I. The extrapolation of the DCS from 5° to 0°, and from 136° to 180° was made by drawing a smooth line through the experimental points, using also the shape of the calculated curves as a guide. The extrapolation error for each transition was found to be (5–8)%. The errors in the integral cross sections listed in Table VI are the root mean square of the errors of Table I, and an 8% extrapolation error.

C. Calibration of the energy and angle scale

The impact energy scale was determined to ±0.1 eV by measuring at $\theta=90°$ the energy location of the He^- $1s2s^2$ resonance at 19.36 eV in our apparatus. A contact potential of 0.4 eV was found, and was added to the nominal kinetic-energy readings to give true incident electron energies of 29.2 ± 0.1 and 39.7 ± 0.1 eV.

The angular scale was calibrated by measuring the symmetry about $\theta=0°$ of elastic scattering from He. A correction of 1° was found, and was the same at the two kinetic energies studied.

III. THEORY

Using the techniques of the many-body field theory, it has been shown[6] that the inelastic T-matrix elements in the static-exchange approximation are given by

$$T(n\vec{q}\tau;o\vec{p}\tau')=\sum_{\sigma_1\sigma_2}\int d\vec{x}\,d\vec{y}\,\{(1/|\vec{x}-\vec{y}|)f_{\vec{q}\tau}^{(-)*}(\vec{x}\sigma_1)\,[f_{\vec{p}\tau'}^{(+)}(\vec{x}\sigma_1)X_n^o(\vec{y}\sigma_2,\vec{y}\sigma_2)-f_{\vec{p}\tau'}^{(+)}(\vec{y}\sigma_2)X_n^o(\vec{y}\sigma_2,\vec{y}\sigma_1)]\}, \quad (1)$$

where o refers to the ground state and $n=(NLM_LSM_S)$ refers to the excited state; $\vec{q}$ and $\vec{p}$ are the wave vectors of the scattered and incident electrons, respectively; τ and τ' are the quantum numbers of the z component of the spin of the scattered and incident electrons, respectively; $\vec{x}$ and $\vec{y}$ are spatial variables; σ_1 and σ_2 are spin variables; $f_{\vec{k}\tau}^{(-,+)}$ is a Hartree-Fock (HF) continuum orbital with momentum $\vec{k}$ of the ground-state target with (incoming, outgoing) boundary conditions; and X_n^o is the target transition density between the ground and excited states computed in the RPA.

Equation (1) is the primary result of FOMBT. It has been applied to the calculation of the He $n=2$ DCS,[7] and the results have been in good agreement with experiment[1-4] for the singlet transitions, and in good-to-qualitative agreement for the triplet transitions. The present work is an extension of the previous theoretical calculations[7] to the $n=3$ excitations. A detailed description of the methods used to evaluate Eq. (1) have been given elsewhere,[12] and only those aspects unique to the $n=3$ transitions will be discussed here.

The RPA transition densities for the $3\,^{1,3}S$ and $3\,^{1,3}P$ states were computed on a Gaussian basis set in Ref. 13, and for the $3\,^{1,3}D$ states on a Slater basis set in Ref. 14. Nine partial waves were sufficient for $f_{\vec{p}}^{(+)}$ and $f_{\vec{q}}^{(-)}$ at the energies studied here for all but the $3\,^1P$ excitation. In this case, 18 partial waves were used: the partial waves $l=0$–8 were computed using HF continuum orbitals, as the theory prescribes, while the partial waves $l=9$–17 were approximated by spherical Bessel functions.

Apart from these computational details, we would like to explore Eq. (1) in somewhat more depth in order to display the plane-wave and distorted-wave contributions to the direct and exchange scattering amplitudes. We will thereby be able to make a clearer comparison in Sec. IV of the FOMBT [Eq. (1)] with other methods[8,9] that have been applied to the e-He system in this energy range. In the course of this comparison, we shall also outline the theoretical origins of the sharp minimum in the $1\,^1S\rightarrow3\,^1S$ DCS (see Fig. 3) in several theoretical approximations.

After factoring in Eq. (1) the spin variables from the scattering orbitals and transition densities, averaging over initial and summing over final spin states, the differential cross section $d\sigma/d\Omega$ may be written as[12]

$$\frac{d\sigma}{d\Omega}(NLM_L S\vec{q};o\vec{p}) = \frac{1}{4\pi^2}\frac{q}{p}\begin{cases}\frac{1}{2}|2T_D - T_E|^2, & S=0 \text{ (singlets)},\\ \frac{3}{2}|T_E|^2, & S=1 \text{ (triplets)},\end{cases} \tag{2}$$

where the direct T_D and exchange T_E amplitudes are

$$T_D = \int d\vec{x}\, d\vec{y}\, f_{\vec{q}}^{(-)*}(\vec{x}) f_{\vec{p}}^{(+)}(\vec{x}) \frac{1}{|\vec{x}-\vec{y}|} X^o_{NLM_LS}(\vec{y},\vec{y}), \tag{3}$$

$$T_E = \int d\vec{x}\, d\vec{y}\, f_{\vec{q}}^{(-)*}(\vec{x}) f_{\vec{p}}^{(+)}(\vec{y}) \frac{1}{|\vec{x}-\vec{y}|} X^o_{NLM_LS}(\vec{y},\vec{x}). \tag{4}$$

The scattering orbitals have the partial-wave expansion

$$f_{\vec{k}}^{(\pm)}(\vec{x}) = \frac{4\pi}{kx}\sum_{lm} i^l \cos\delta_l(k) e^{\pm i\delta_l(k)} \times u_l(k,x) Y^*_{lm}(\hat{k}) Y_{lm}(\hat{x}), \tag{5}$$

where δ_l is the phase shift of the lth partial wave, Y_{lm} the spherical harmonics, and where the radial functions u_l are solutions of the integral equation

$$u_l(k,x) = kx\, j_l(kx) + \int\int G_l(x,x_1) V_l^{\mathrm{HF}}(x_1,x_2) \times u_l(k,x_2)\, dx_1\, dx_2. \tag{6}$$

Here, j_l is a spherical Bessel function, V_l^{HF} is the HF potential, and G_l is the free-wave Green's function.[15]

The details of calculating the radial functions u_l and the phase shifts δ_l may be found in Ref. 15. For our purposes, in order to compare for the singlet transitions the results of the present calculations with the results of the Born approximation, it is sufficient to note that when the second term in Eq. (6) is ignored, and the phase shifts set to zero, $f_{\vec{k}}^{(\pm)}$ becomes a plane-wave $e^{i\vec{k}\cdot\vec{x}}$. Equation (3) then becomes the expression for the Born T matrix. It may be seen, then, that the FOMBT differs from a partial-wave Born calculation in that the FOMBT contains (i) "plane-wave" terms modulated by the nonzero phase shifts through the factors $\cos\delta_l e^{i\delta_l}$ [Eq. (5)], (ii) an additional "distorted-wave" term arising from the second term in Eq. (6), and (iii) an exchange amplitude [Eq. (4)]. Equation (4) differs from the Born-Oppenheimer exchange term in that the core term $1/x$ is missing from the transition potential in the FOMBT, and the f's are distorted waves. Therefore, when the f's are plane waves, Eq. (4) gives the Born-Oppenheimer-minus-core (BOMC) approximation. This approximation has been discussed previously.[16]

Equation (1) is a distorted-wave (DW) formula. It would result from the first-order Kohn correction to a diagonal trial matrix of solutions (orthogonal to bound orbitals) of the close-coupling equations,[17,18] using also the RPA for the transition densities. However, DW theory leaves the choice of trial functions arbitrary, and these trial functions are usually computed by completely decoupling the close-coupling equations. This procedure involves computing the orbital of the outgoing electron in the field of the *excited* state. In the FOMBT, the orbital is computed in the field of the *ground* state, with proper outgoing momentum q. This choice was introduced in Ref. 19 to achieve orthogonality between the orbital of the incoming and outgoing electron.

Physically, the difference lies in the two assumptions that the scattered electron either leaves the potential range in a time that is *short* relative to the time it takes the target to undergo its excitation (FOMBT), or that the target is excited *rapidly* with respect to the transit time of the electron, so that the outgoing electron "sees" only the potential of the excited state (DW theory). In actual fact, while the electron is within the range of the target potential, the target will be in some intermediate dynamic state. Which of the two times—excitation or electron transit—will be shorter, can, at present, only be judged by an appeal to experimental results at an energy where other effects, such as polarization and short-range correlation (coupling to other channels), are small. However, previous experience gained through studies of the $n=2$ excitations of He,[19] and of the $2s$ and $2p$ excitations of the H atom[20] have shown that at intermediate energies (approximately 5–100 eV above the ionization threshold), computing $f_{\vec{q}}^{(-)}$ in the field of the *ground* state gives superior results. In other words, the electron transit time is, in reality, rapid with respect to the target excitation time. This heuristic, but physically appealing two-time model has also been discussed in Ref. 21.

IV. RESULTS AND DISCUSSION

The intensity ratios for scattering into the $n=3$ states of helium relative to scattering into the $2\,^3P$ and $2\,^1P$ states are listed in Tables II and III at 29.2 eV and 39.7 eV, respectively. The experi-

TABLE II. Scattering intensity ratios of the $n=3$ transitions to the $2\,^1P$ and $2\,^3P$ states at $E_0=29.2$ eV.

θ (deg)	$3\,^3S$ to $2\,^3P$	$3\,^3S$ to $2\,^1P$	$3\,^1S$ to $2\,^3P$	$3\,^1S$ to $2\,^1P$	$3\,^3P$ to $2\,^3P$	$3\,^3P$ to $2\,^1P$	$3\,^1P, 3\,^{1,3}D$ to $2\,^3P$	$3\,^1P, 3\,^{1,3}D$ to $2\,^1P$
5	0.44	0.016	2.0	0.071	0.33	0.012	4.3	0.15
10	•••	0.018	•••	0.061	•••	0.010	•••	0.17
20	0.27	0.021	0.61	0.048	0.13	0.011	2.2	0.17
30	0.22	0.036	0.15	0.025	0.15	0.025	1.3	0.22
35	0.26	0.057	0.11	0.024	0.18	0.039	1.4	0.30
40	•••	•••	•••	0.0086	•••	0.056	•••	0.28
45	0.17	0.11	•••	0.0085	0.14	0.087	0.37	0.26
50	•••	•••	•••	0.014	•••	0.13	•••	0.26
55	•••	•••	•••	0.041	•••	0.17	•••	0.30
60	0.22	0.36	0.035	0.058	0.15	0.25	0.19	0.31
68	•••	•••	•••	0.086	•••	0.32	•••	0.25
75	0.27	0.59	0.042	0.090	0.16	0.35	0.14	0.30
90	0.23	0.57	•••	0.13	0.21	0.58	0.12	0.33
100	0.20	0.61	0.062	0.20	0.23	0.72	0.12	0.37
105	0.14	0.48	0.080	0.28	0.20	0.70	0.097	0.34
112	0.081	0.29	0.11	0.39	0.22	0.79	0.094	0.33
120	0.039	0.15	0.17	0.64	0.26	0.98	0.097	0.37
128	0.047	0.16	0.22	0.76	0.24	0.85	0.12	0.41
136	0.067	0.21	0.26	0.81	0.27	0.86	0.13	0.39

mental and theoretical DCS are listed in Tables IV and V for the two energies, and are plotted in Figs. 2–10.

The integral cross sections Q are listed in Table VI. Also listed are the optical excitation-function measurements of Q for the $3\,^3P$ transition,[22] the $3\,^1P$ transition,[5] and the $3\,^{1,3}S$, $3\,^3P$, and $3\,^{1,3}D$ transitions[23]; and calculated Q for the $3\,^1S$, $3\,^1D$, and $3\,^1P$ transitions,[8] and the $3\,^3S$ transition.[9]

Several interesting trends emerge in both the experimental and theoretical results when the present work is compared to the results for the $n=2$ transitions. In this section we shall make a state-by-state comparison of the experimental and theoretical DCS for the $n=3$ and $n=2$ transitions in order to identify the trends and differences in the measurements and calculations for the two Rydberg manifolds.

A. Transitions

1. $3\,^1S$

The measured and computed DCS for the excitation to the $3\,^1S$ state are listed in Tables IV and V,

TABLE III. Scattering intensity ratios of the $n=3$ transitions to the $2\,^1P$ and the $2\,^3P$ states at $E_0=39.7$ eV.

θ (deg)	$3\,^3S$ to $2\,^3P$	$3\,^3S$ to $2\,^1P$	$3\,^1S$ to $2\,^3P$	$3\,^1S$ to $2\,^1P$	$3\,^3P$ to $2\,^3P$	$3\,^3P$ to $2\,^1P$	$3\,^1P, 3\,^{1,3}D$ to $2\,^3P$	$3\,^1P, 3\,^{1,3}D$ to $2\,^1P$
5	0.90	0.0077	5.2	0.045	0.57	0.0049	21	0.18
10	0.76	0.0087	2.9	0.033	•••	•••	15	0.17
15	0.52	0.012	1.3	0.029	0.37	0.0086	9.0	0.21
20	0.37	0.015	0.57	0.023	0.28	0.011	5.6	0.23
25	•••	•••	•••	0.012	•••	0.017	•••	0.25
30	0.17	0.031	0.031	0.0056	0.19	0.036	1.4	0.25
45	0.064	0.053	•••	0.012	0.18	0.14	0.25	0.23
60	0.059	0.075	•••	0.012	0.20	0.27	0.21	0.28
75	0.065	0.088	•••	0.021	0.19	0.29	0.20	0.27
90	0.063	0.080	0.11	0.14	0.24	0.31	0.19	0.24
105	0.035	0.058	0.22	0.36	0.30	0.45	0.20	0.30
110	0.037	0.072	0.22	0.40	0.28	0.48	0.18	0.30
120	0.089	0.14	0.29	0.44	0.28	0.44	0.17	0.26
136	0.33	0.44	0.77	1.0	0.31	0.41	0.25	0.33

TABLE IV. Absolute experimental and theoretical differential cross sections, in units of 10^{-20} cm^2/sr, for excitation to the $n=3$ states of He at $E_0=29.2$ eV. Experimental values in parentheses are extrapolated values. The theoretical DCS are calculated in the first-order many-body theory.

θ	$3\,^3S$		$3\,^1S$		$3\,^3P$		$3\,^1P, 3^{1,3}D$		$3\,^1P$	$3\,^3D$	$3\,^1D$
(deg)	Expt.	Theor.	Expt.	Theor.	Expt.	Theor.	Expt.	Theor.	Theor.	Theor.	Theor.
0	(9.8)	9.4	(50)	8.4	(7.8)	22	(100)	63	56	5.3	1.7
5	9.1	9.3	41	8.2	6.9	22	87	61	54	5.3	1.7
10	8.1	9.0	27	7.7	4.5	22	70	55	48	5.2	1.6
20	4.4	8.0	9.9	5.9	2.1	21	35	40	34	4.8	1.2
30	3.5	6.7	2.4	3.8	2.4	20	21	26	21	4.2	0.83
35	3.7	6.0	1.6	2.8	2.6	19	20	19	15	3.8	0.64
40	•••	5.4	0.34	1.9	2.2	18	11	15	11	3.4	0.48
45	3.1	4.8	0.24	1.1	2.5	17	7.0	11	7.4	3.0	0.36
50	•••	4.2	0.26	0.59	2.4	16	4.8	8.0	5.1	2.6	0.27
55	•••	3.8	0.57	0.23	2.4	15	4.2	5.9	3.4	2.3	0.22
60	3.8	3.4	0.61	0.041	2.6	14	3.3	4.6	2.4	2.0	0.18
68	•••	3.0	0.71	0.052	2.6	14	2.1	3.3	1.5	1.6	0.17
75	4.2	2.8	0.65	0.29	2.5	14	2.2	2.7	1.1	1.4	0.17
90	3.4	2.6	0.83	1.2	3.4	15	2.0	2.2	0.82	1.2	0.21
100	3.6	2.6	1.2	1.9	4.2	18	2.2	2.5	0.76	1.5	0.25
105	2.8	2.7	1.6	2.2	4.0	19	2.0	2.5	0.74	1.5	0.27
112	1.7	2.9	2.3	2.6	4.7	21	2.0	2.6	0.70	1.6	0.30
120	0.88	3.1	3.8	3.1	5.8	24	2.2	2.8	0.66	1.8	0.33
128	0.93	3.3	4.4	3.4	4.9	27	2.4	3.0	0.63	2.0	0.37
136	1.3	3.5	4.9	3.8	5.2	30	2.4	3.3	0.60	2.3	0.40
145	(1.6)	3.9	(5.2)	4.0	(5.6)	32	(2.5)	3.5	0.59	2.5	0.44
150	(1.9)	4.0	(5.4)	4.2	(5.8)	33	(2.6)	3.6	0.58	2.6	0.45
160	(2.0)	4.3	(5.6)	4.4	(5.8)	35	(2.6)	3.8	0.57	2.8	0.48
170	(2.1)	4.4	(5.7)	4.5	(5.9)	36	(2.6)	4.0	0.56	2.9	0.50
180	(2.1)	4.5	(5.7)	4.5	(5.9)	37	(2.7)	4.0	0.56	2.9	0.50

TABLE V. Absolute experimental and theoretical differential cross sections, in units of 10^{-20} cm^2/sr, for excitation to the $n=3$ states of He at $E_0=39.7$ eV. Experimental values in parentheses are extrapolated values. The theoretical DCS are calculated in the first-order many-body theory.

θ	$3\,^3S$		$3\,^1S$		$3\,^3P$		$3\,^1P, 3\,^{1,3}D$		$3\,^1P$	$3\,^3D$	$3\,^1D$
(deg)	Expt.	Theor.	Expt.	Theor.	Expt.	Theor.	Expt.	Theor.	Theor.	Theor.	Theor.
0	(17)	6.2	(110)	25	(11)	40	(410)	331	316	5.6	9.3
5	16	6.0	91	24	10	40	370	312	297	5.5	9.1
10	14	5.6	53	22	•••	39	280	262	248	5.4	8.3
15	10	4.9	26	19	7.3	39	180	198	186	5.2	7.1
20	7.1	4.2	11	15	5.3	37	110	140	129	5.0	5.6
25	•••	3.4	3.2	12	4.6	36	68	93	84	4.6	4.0
30	4.6	2.6	0.83	8.3	5.2	34	37	60	53	4.2	2.7
45	1.9	1.1	0.46	1.8	5.3	26	8.0	14	11	2.6	0.65
60	1.1	0.54	0.18	0.45	3.9	16	4.0	4.8	3.2	1.4	0.23
75	0.84	0.59	0.20	1.4	2.6	10	2.6	3.1	2.2	0.72	0.17
90	0.63	1.1	1.1	2.5	2.4	8.9	1.9	2.7	2.0	0.52	0.15
105	0.36	2.0	2.3	3.4	3.0	9.4	2.0	2.5	1.8	0.55	0.14
110	0.40	2.3	2.3	3.7	2.8	10	1.8	2.4	1.7	0.59	0.15
120	0.83	3.2	2.7	4.1	2.6	11	1.6	2.4	1.6	0.68	0.15
136	2.6	4.5	5.9	4.5	2.4	14	1.9	2.5	1.5	0.82	0.17
145	(3.0)	5.3	(6.9)	4.7	(2.2)	15	(1.8)	2.6	1.5	0.88	0.18
150	(3.1)	5.7	(7.6)	4.8	(2.2)	15	(1.8)	2.6	1.5	0.91	0.19
160	(3.6)	6.3	(8.5)	4.9	(2.1)	16	(1.8)	2.6	1.5	0.94	0.20
170	(3.8)	6.6	(9.0)	5.0	(2.1)	16	(1.8)	2.7	1.5	0.96	0.21
180	(3.9)	6.8	(9.4)	5.0	(2.1)	17	(1.8)	2.7	1.5	0.96	0.21

TABLE VI. Integral cross sections Q (in 10^{-19} cm^2) for excitation of the $n=3$ transitions in He by electron impact at $E_0 = 29.2$ and 39.7 eV.

State	Method	Q Expt. 29.2 eV	Q Expt. 39.7 eV	Q Calc. 29.2 eV	Q Calc. 39.7 eV
$3\,^3S$	This work	3.8 ± 0.9	2.4 ± 0.6	4.7	3.0
	Reference 23	5.4	6.9		
	Reference 9			12	6.1
$3\,^1S$	This work	3.5 ± 1.1	4.4 ± 1.4	2.8	4.8
	Reference 23		~4.7		
	Reference 8 (B/BOR) [a]			190/370	170/260
3^3P	This work	4.7 ± 1.1	4.1 ± 0.9	26	20
	Reference 22	5.4 ± 1.1	4.7 ± 1.0		
	Reference 23	4.2	6.7		
$3\,^1P, 3^{1,3}D$	This work	7.6 ± 1.8	15.9 ± 3.8	8.7	19
	Sum of individually measured Q's below	10	21		
$3\,^1P$	This work			5.5	17
	Reference 8 (B/BOR) [a]			24/34	34/37
	Reference 5	7.3 ± 0.7	15.3 ± 1.5		
$3\,^3D$	This work			2.7	1.7
	Reference 23	1.3	2.1		
$3\,^1D$	This work			0.46	0.81
	Reference 8 (B/BOR) [a]			1.1/1.6	1.3/1.5
	Reference 23	1.6	3.3		

[a] Calculations of Ref. 8 carried out in the Born (B) and Born-Ochkur-Rudge (BOR) approximations.

and shown in Figs. 2 and 3. The shapes and trends are somewhat the same as for the $2\,^1S$ transition.[1,3,7] At 29.2 eV (Fig. 2), the experiment shows a steep minimum at 45°, a plateau between 60° and 90°, and a rise thereafter. At 39.7 eV (Fig. 3), the plateau has nearly disappeared, and the minimum has broadened and shifted to higher scattering angles.

The calculated curve at 29.2 eV lies below experiment at angles less than 30°, has a minimum which is too deep, and which lies at larger angles than experiment. It also lacks the plateau seen experimentally at angles between 60° and 90°. The calculation at 39.7 eV again lies below experiment at low angles, less than 20°, but otherwise has the same general shape. In magnitude, it is a factor of 1–4 that of experiment in the angular range 20°–136°.

The origin of the sharp minimum in the $3\,^1S$ DCS (and also in the $2\,^1S$ DCS, see Refs. 1, 3, and 7) is intriguing. Recent calculations in the post-Ochkur approximation[8] have also yielded a sharp minimum in the $3\,^1S$ DCS, and it is interesting to explore the cause of the minimum structure in the two theories. As pointed out in Sec. III, the FOMBT scattering amplitudes differ from the partial-wave Born amplitudes in that the former (i) are modulated by nonzero phase shifts, (ii) contain an additional "distorted-wave" term, and (iii) contain an exchange amplitude. The relative importance of (i) and (ii) will be the subject of a future investigation.[24] However, for the present purposes, one may compute the direct and exchange contributions to the DCS by setting T_E and T_D, respectively, equal to zero in Eq. (2). The resulting individ-

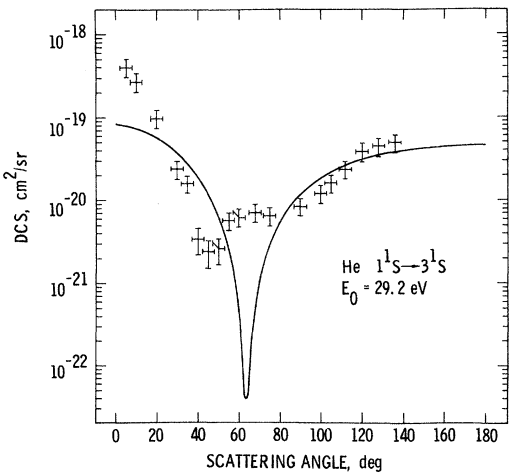

FIG. 2. Measured normalized absolute differential scattering cross sections for the transition $1\,^1S \rightarrow 3\,^1S$ in helium at $E_0 = 29.2$ eV. The solid line is the differential cross section calculated in the first-order many-body theory (FOMBT).

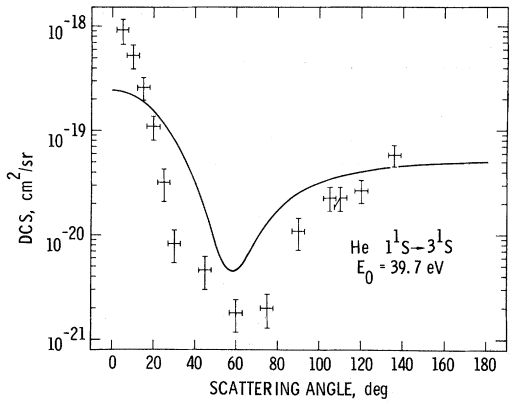

FIG. 3. Same as in Fig. 2, but at $E_0 = 39.7$ eV.

ual contributions to the $1\,^1S \rightarrow 3\,^1S$ DCS at 39.7 eV are shown in Fig. 4, where the DCS calculated in the Born and post-Ochkur approximations[8] are also shown. Two interesting facts emerge from Fig. 4: that (i) and/or (ii) above are responsible for the good agreement of the FOMBT with experiment; and second, that the FOMBT exchange amplitude makes only a small contribution to the total amplitude. This is a sharp contrast to the Ochkur-like plane-wave theories[25] which can only correct the large Born cross section through an added large exchange amplitude.

Of the several approximations discussed in Ref. 25, only the post-Ochkur results[8] gave rise to a minimum in the same angular range as experiment. This minimum at 39.7 eV (Fig. 4) was, however, much sharper than either the experimental minimum or the FOMBT results. Moreover, a similar minimum was found in the $3\,^1P$ DCS in the post-Ochkur calculation[8] at 39.7 eV where no experimental (Fig. 8) or theoretical [Eq. (1)] minimum exists (see also Sec. IV A3). The applicability of the post-Ochkur treatment to the e-He system thus appears to be questionable at these electron energies.

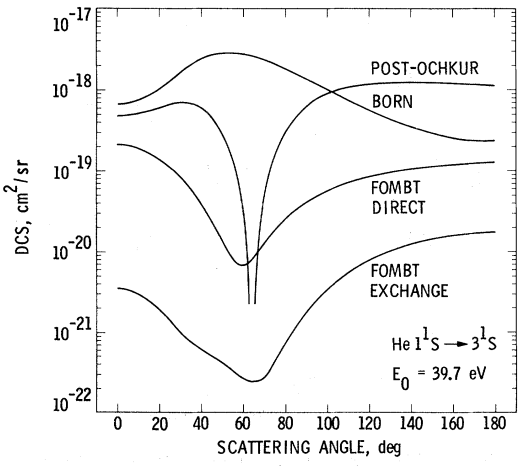

FIG. 4. Comparison of the DCS for the $1\,^1S \rightarrow 3\,^1S$ transition at 39.7 eV as calculated in the Born and post-Ochkur theories (Ref. 8), with the direct and exchange contributions to the DCS as calculated in the FOMBT.

At 29.2 eV (Fig. 2) the agreement between the FOMBT and experiment is not as good as in the $2\,^1S$ case.[7] In the present work the theoretical minimum lies near 60° with a minimum cross section of 4×10^{-23} cm²/sr, while the experimental minimum lies near 45° with a minimum cross section of 2.4×10^{-21} cm²/sr—a factor 60 that of theory. One may argue that the reason for the larger experimental cross section is that with the finite angular resolution of the spectrometer (approximately ±3°, see Ref. 1) one always observes *some* scattering from regions of larger cross section. A sharp (in angle) minimum such as that predicted by theory would necessarily be broadened by the finite spatial resolution of the spectometer. However, one would expect the location, in angle, of the experimental and theoretical minima to be very nearly the same from this angular-resolution argument. Such is not the case.

In view of the above analysis, a more likely explanation for the sharp theoretical minimum is that polarization effects may be more important for the $3\,^1S$ excitation at the lower energy. For example, the inclusion of polarization in the scattering orbital, such as in the second-order MBT,[26] will add a third term of the form $\int GV^{\rm pol}u$ to Eq. (6), where $V^{\rm pol}$ is the polarization potential. This term gives rise to the possibility of additional interferences being superimposed on the first-order (static-exchange) effect.

2. $3\,^3S$

The experimental and theoretical DCS for the $1\,^1S \rightarrow 3\,^3S$ transition are listed in Tables IV and V, and shown in Figs. 5 and 6. The shapes of the experimental curves are very similar to those of the $2\,^3S$ transition at 29.6 and 40.1 eV.[1,3] At the lower energy (Fig. 5), the experimental DCS shows a minimum at $\theta \sim (40\text{–}50)°$, a rise in the range (60–90)°, a second deeper minimum near 120°, and a rise thereafter. Only one broad minimum appears at 39.7 eV near 100° (Fig. 6). The computed DCS's agree qualitatively with the experiments in magnitude, and in following the trend of deeper minimum at higher energies.

The only other calculation for this state is that of Ref. 9 at 40.1 eV. There, a Born-Oppenheimer calculation with a modified s-wave amplitude was carried out. The resultant DCS gave a deep, narrow minimum between 50° and 60°. The qualitative behavior of the minimum was insensitive to ener-

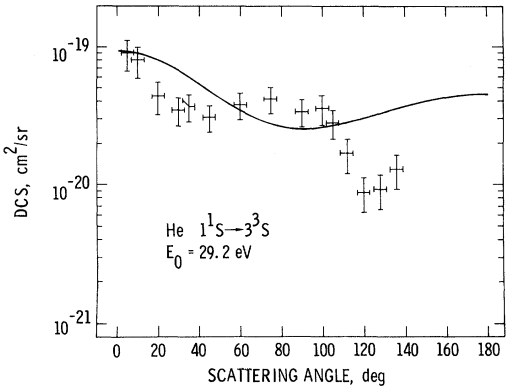

FIG. 5. Same as in Fig. 2, but for the $1^1S \rightarrow 3^3S$ transition.

gy, and remained in the 2^3S transition even at 200 eV, long after it had disappeared from experiments (see Fig. 5 of Ref. 9). This minimum very likely arises from an underestimation of the s-wave amplitude.[24] As in the 3^1S case, we feel that the static-exchange effect is dominant, and is properly described in the FOMBT. We also feel that inclusion of polarization effects will bring out the finer details of the experimental structure, such as the double-minimum structure in Fig. 5. As justification for this, we note that polarization was included in a preliminary calculation[27] of the 2^3S DCS at 29.6 eV through coupling of the 1^1S and $n=2$ manifold states, including also a many-channel optical potential. The resultant DCS showed the double-minimum behavior[27] to be in good agreement with experiment.[1,3]

3. 3^1P and $3^{1,3}D$

As noted in Sec. II, the 3^1P transition lies only 0.014 and 0.013 eV away from the 3^3D and 3^1D transitions, respectively, so that the ^1P and $^{1,3}D$

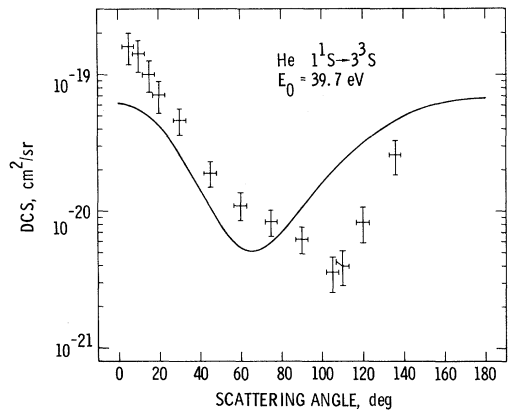

FIG. 6. Same as in Fig. 5, but at $E_0 = 39.7$ eV.

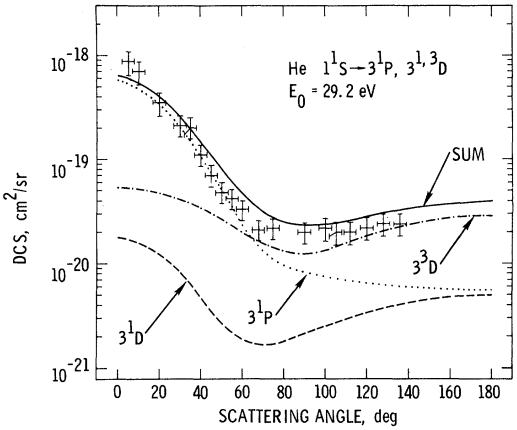

FIG. 7. Same as in Fig. 2, but for the combined $1^1S \rightarrow 3^1P$, $3^{1,3}D$ transitions. The calculated differential cross sections of each of the individual transitions are shown, as well as their sum.

states could not be resolved in the present work. As seen in Figs. 7 and 8, the combined transitions exhibit the same forward peaking in the DCS as was seen in the $n=2$ case.[1,3] However, one observes in Fig. 7 an unusual rise in the experimental DCS at angles greater than about 80°, rather than the steady decrease which one would expect for a pure ^1P transition. The reason for this rise becomes evident when the theoretical results for the 3^1P, 3^1D, and 3^3D DCS are examined separately. From the individual DCS displayed in Fig. 7, one sees that the main contribution in the forward direction, at angles less than ~60°, arises from the 3^1P transition. At larger angles the DCS of the 3^1P state drops smoothly while the 3^3D DCS increases until it comprises ~80% of the total DCS (labeled "sum" in Fig. 7) at

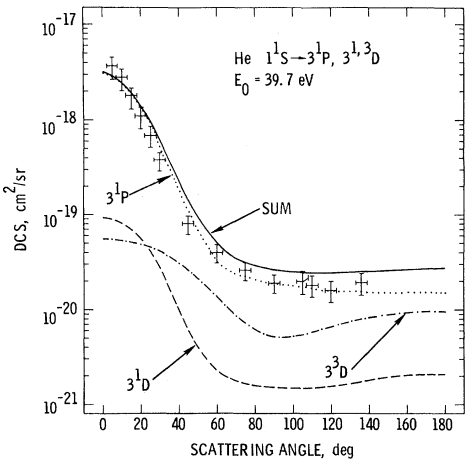

FIG. 8. Same as in Fig. 7, but at $E_0 = 39.7$ eV.

$\theta = 136°$. At 39.7 eV (Fig. 8) the DCS of the ^3D state is less than that of the ^1P state. It comprises only 30% of the total DCS at 136°, and one observes only a flattening of the DCS starting at $\theta \sim 80°$, rather than a rise (increasing ^3D contribution) or a steady decrease (pure $3\,^1P$). At both energies the $3\,^1D$ transition is calculated to contribute, at most, 12% to the total DCS, and may thus be neglected in these arguments.

Also of interest in Figs. 7 and 8 is the fact that at angles less than ~60°, where the ^3D transition does not contribute significantly, the agreement between experiment and theory is excellent. The generally smaller theoretical DCS at angles near 0° is again very likely due to neglect of the polarization in the transition potential.[7] At larger angles, it should be pointed out, in fairness, that at the lower energy the FOMBT is known to underestimate the ^1P DCS,[7] and to overestimate triplet-state DCS's at all angles. Therefore, while the calculation undoubtedly provides the correct explanation for the rise in the DCS at high angles, the fact that experimental accuracy appears to have been achieved is very likely due to the sum of a ^1P DCS which is an underestimate and a ^3D DCS which is an overestimate.

The shape of the $3\,^1P$ DCS calculated in the Born approximation[8] paralleled the experimental results at angles less than 60°, but was 2–4 times that of experiment in magnitude. Inclusion of Ochkur-like exchange terms gave some improvement in this angular region. A notable exception was the post-Ochkur approximation which gave a sharp minimum at 30°, similar to the minimum shown for the $3\,^1S$ transition in Fig. 4. At angles greater than 60°, the DCS calculated in the Born and Ochkur-like approximations[8] continued to decrease steadily, in disagreement with experiment and the FOMBT.

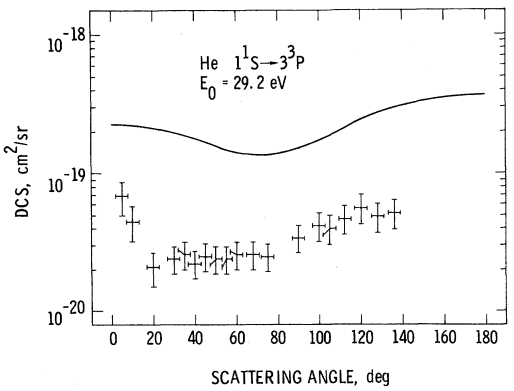

FIG. 9. Same as in Fig. 2, but for the $1\,^1S \rightarrow 3\,^3P$ transition.

4. $3\,^3P$

Experimentally, the $3\,^3P$ DCS at 29.2 eV (Fig. 9) is slightly peaked in the forward direction, passes through a shallow, broad minimum between 20° and 75°, and rises in the backward direction. At 39.7 eV (Fig. 10) the DCS drops steadily with increasing θ, with evidence for several small oscillations. A similar qualitative behavior was observed in the $2\,^3P$ experimental DCS.[1,3] The FOMBT provides the correct general shape of the $3\,^3P$ DCS but, as in the $n = 2$ case,[7] fails to account for the oscillations, and gives cross sections which are factors of 3–6 too large at both energies.

In general, triplet-state cross sections suffer most in this first-order theory since triplet states may only couple to the ground state through a nonlocal exchange potential. However, it is not clear why the $3\,^3P$ DCS should be in worse agreement with experiment than that of the $3\,^3S$ transitions (see Figs. 5 and 6).

B. Integral cross sections

The differential cross sections of Figs. 2, 3, 5–10 were extrapolated to $\theta = 0°$ and 180°, and the set of data, each point multiplied by the factor $2\pi \sin\theta$, was fitted by the method of cubic splines. The resulting cubic-fit polynomial was then easily integrated to give the results for the integral cross sections Q listed in Table VI. Also listed in Table VI are the theoretical calculations[8] for the $3\,^1S$, $3\,^1P$, and $3\,^1D$ states, and the $3\,^3S$ state[9]; the optical excitation-function measurements of Ref. 23; the measurements of Ref. 22 for the $3\,^3P$ state; and the measurements of Ref. 5 for the $3\,^1P$ state. The Q's from the measurements of Ref. 23 were obtained by reading as accurately as possible the values in Fig. 2 of that paper. The measurements of the $3\,^3P$ and $3\,^1P$ states were derived by drawing smooth curves through the values of Q listed in

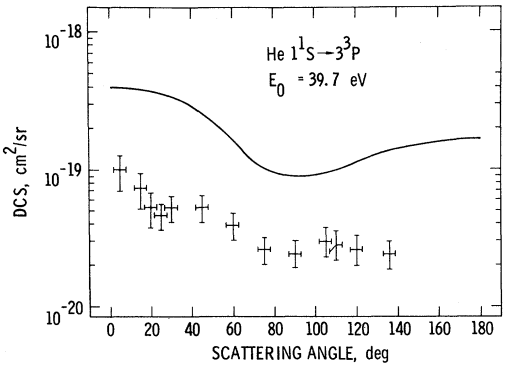

FIG. 10. Same as in Fig. 9, but at $E_0 = 39.7$ eV.

Refs. 22 and 5, respectively, and obtaining the values at the intermediate energies of 29.2 and 39.7 eV. No other measurements of the integral cross sections could be found in the literature in the energy-range threshold to 50 eV, although there are experimental and theoretical data at $E_0 \geq 50$ eV.[28] Because the integral cross sections are changing rapidly with E_0 between threshold and 50 eV[23] we have listed in Table VI only those experiments and calculations which were carried out near the energies of the present work.

The agreement in Table VI between the FOMBT and the present experiments is again excellent, as was true for the $n=2$ case.[7] Agreement is within experimental error for all but the $3\,^3P$ transition. Here theory overestimates the integral cross section for the same reasons discussed in Sec. IV A4 with regard to the differential cross section. It is interesting to note that even for this state the theory correctly reproduces the experimental trend of decreasing Q with increasing E_0.

Also of interest is the fact that the experimental sum of the *individual* $3\,^3D$, $3\,^1D$, and $3\,^1P$ Q's at both incident energies is greater than the combined measurement of the present work. The measurements of Ref. 23 for the $3\,^{1,3}D$ Q give a total of $\sim 5.4\times10^{-19}$ cm^2 at 39.7 eV. In the extreme case (assuming the lowest value of Q for the $3\,^1P$ state from Ref. 5, and the highest value of the sum in the present work) the $3\,^{1,3}D$ cross sections could be at most $\sim 5.9\times10^{-19}$ cm^2, and probably much less than this. The same argument applies at 29.2 eV, where the upper limit is 2.8×10^{-19} cm^2. It thus appears that the measurements of Ref. 23 for these states are too high. The same tendency in the measurements[23] is observed in the $3\,^3S$ and $3\,^3P$ Q at 29.7 eV. In the $3\,^3P$ case, the present measurements are in good agreement with those of Ref. 22 at the two energies.

ACKNOWLEDGMENTS

We thank Professor V. McKoy for the RPA transition densities of the $3\,^{1,3}S$ and $3\,^{1,3}P$ states, and Dr. B. S. Yarlagadda for the RPA transition densities of the $3\,^{1,3}D$ states. We also thank Professor D. G. Truhlar for providing us with differential and integral cross sections calculated in the Born and several Ochkur-like approximations for the ^1S, ^1P, and ^1D states. One of us (A. C.) thanks Dr. S. Trajmar for his encouragement of this work, and Dr. Gy. Csanak for pointing out the importance of a theoretical and experimental study of the $n=3$ transitions in helium. We also thank Professor Truhlar, Dr. Trajmar, Dr. Csanak, and Dr. R. K. Nesbet for their valuable comments on this paper. We gratefully acknowledge support from the Caltech President's Fund, the National Aeronautics and Space Administration through Contract No. NAS7-100 to the Jet Propulsion Laboratory, and the Office of Naval Research under Contract No. N00014-72-C-0051.

[1]S. Trajmar, Phys. Rev. A 8, 191 (1973).
[2]D. G. Truhlar, S. Trajmar, W. Williams, S. Ormonde, and B. Torres, Phys. Rev. A 8, 2475 (1973).
[3]R. I. Hall, G. Joyez, J. Mazeau, J. Reinhardt, and C. Schermann, J. Phys. (Paris) 34, 827 (1973).
[4]C. B. Crooks, R. D. DuBois, D. E. Golden, and M. E. Rudd, Phys. Rev. Lett. 29, 327 (1972).
[5]F. G. Donaldson, M. A. Hender, and J. W. McConkey, J. Phys. B 5, 1192 (1972).
[6]Gy. Csanak, H. S. Taylor, and R. Yaris, Adv. At. Mol. Phys. 7, 287 (1971).
[7]L. D. Thomas, Gy. Csanak, H. S. Taylor, and B. S. Yarlagadda, J. Phys. B 7, 1719 (1974).
[8]D. G. Truhlar (private communication).
[9]K. C. Mathur and M. R. H. Rudge, J. Phys. B 7, 1033 (1974).
[10]A. Chutjian, J. Chem. Phys. 61, 4279 (1974).
[11]D. C. Cartwright and N. A. Fiamengo (private communication).
[12]L. D. Thomas, B. S. Yarlagadda, Gy. Csanak, and H. S. Taylor, Comput. Phys. Commun. 6, 316 (1974).
[13]V. McKoy (private communication).
[14]B. S. Yarlagadda, Gy. Csanak, H. S. Taylor, B. Schneider, and R. Yaris, Phys. Rev. A 7, 146 (1973).
[15]L. D. Thomas, J. Comp. Phys. 13, 348 (1973).
[16]D. G. Truhlar, D. C. Cartwright, and A. Kuppermann, Phys. Rev. 175, 173 (1968); J. C. Steelhammer, Ph.D. Thesis (University of Minnesota, 1971) (unpublished).
[17]I. Percival and M. J. Seaton, Proc. Camb. Philos. Soc. 53, 645 (1957).
[18]W. Eissner and M. J. Seaton, J. Phys. B 5, 2187 (1972).
[19]D. H. Madison and W. N. Shelton, Phys. Rev. A 7, 499 (1973).
[20]M. S. Pindzola and H. P. Kelly, Phys. Rev. A 11, 221 (1975).
[21]H. S. Taylor, A. Chutjian, and L. D. Thomas, *International Symposium on Electron and Photon Interactions with Atoms, University of Stirling, Stirling, Scotland, 1974* (Plenum, New York, to be published).
[22]J. W. McConkey and J. M. Woolsey, in *Abstracts of the Sixth International Conference on the Physics of Electronic and Atomic Collisions, Cambridge, Mass.* (MIT Press, Cambridge, Mass., 1969), p. 355.
[23]R. M. St. John, F. L. Miller, and C. C. Lin, Phys. Rev. 134, A888 (1964).
[24]L. D. Thomas (to be published).
[25]D. G. Truhlar, J. K. Rice, A. Kuppermann, S. Trajmar, and D. C. Cartwright, Phys. Rev. A 1, 778 (1970).
[26]Gy. Csanak, H. S. Taylor, and D. N. Tripathy, J. Phys. B 6, 2040 (1973).

[27]L. D. Thomas and R. K. Nesbet, Abstracts of the Fourth International Conference on Atomic Physics, Heidelberg, West Germany, 1974 (unpublished).

[28]See, for example, Ref. 5 above and references cited therein ($3\,^1P$); D. Baye and P. -H. Heenen, J. Phys. B 7, 938 (1974) ($3\,^1S$, $3\,^1D$, $3\,^1P$); A. F. J. van Raan, P. G. Moll, and J. van Eck, J. Phys. B 7, 950 (1974) ($3\,^3P$); R. J. Anderson, R. H. Hughes, J. H. Tung, and S. T. Chen, Phys. Rev. A 8, 810 (1973) ($3\,^3P$); K. L. Bell, D. J. Kennedy, and A. E. Kingston, J. Phys. B 1, 204 (1968) ($3\,^1P$, $3\,^1D$, theoretical, first Born); S. P. Ojha and P. Tiwari, J. Chem. Phys. 59, 5676 (1972) and S. P. Ojha, P. Tiwari, and D. K. Rai, J. Phys. B 5, 2231 (1972) ($3\,^3P$, theoretical, Ochkur); S. P. Ojha, P. Tiwari, and D. K. Rai, Can. J. Phys. 51, 311 (1973) ($3\,^1P$, theoretical, first Born); F. T. Chan and S. T. Chen, Phys. Rev. A 10, 1151 (1974) ($3\,^1P$, theoretical, Glauber).